Uncovering Network Architecture Using an Exact Statistical Input-Output Relation of a Neuron Model

Safura Rashid Shomali[1,*], Majid Nili Ahmadabadi[2,1], Seyyed Nader Rasuli[3,4], Hideaki Shimazaki[5,6]

1 School of Cognitive Sciences, Institute for Research in Fundamental Sciences (IPM), Tehran 19395-5746, Iran

2 Control and Intelligent Processing Center of Excellence, School of Electrical and Computer Engineering, College of Engineering, University of Tehran, Tehran 14395-515, Iran

3 Department of Physics, University of Guilan, Rasht 41335-1914, Iran

4 School of Physics, Institute for Research in Fundamental Sciences (IPM), Tehran 19395-5531, Iran

5 Graduate School of Informatics, Kyoto University, Sakyo-ku, Kyoto 606-8501, Japan

6 Honda Research Institute Japan, Wako-shi, Saitama, 351-0188, Japan

* safura@ipm.ir

Abstract

Identifying network architecture from recorded neural activity is one of the major challenges in neuroscience. A key requirement for this challenge is the knowledge of the statistical input-output relation of single neurons operating under in vivo conditions. However, lack of analytical representation even for a standard neuron model prohibited theoretical investigations. Recently we provided an exact analytical solution of spike-timing for a leaky integrate-and-fire (LIF) neuron responding to synaptic inputs under noisy background input balanced near the threshold [Shomali *et. al.*, J Comput Neurosci 44, (2018): 147]. Using that solution, we construct a unified framework that links synaptic inputs, nonlinearity of spiking, network architecture, and statistics of population activity. With this approach, we theoretically predict correlated population activity of in vivo neurons that receive common inputs under different network architectures. It allows us to present a quantitative method to unveil the network architecture behind the sparse population activity ubiquitously observed in visual and hippocampal neurons. We show that two motifs can disclose this activity: Inhibitory common inputs to three (or more)

neurons or excitatory common inputs to pairs of neurons. By comparing model prediction with empirical observation of monkey V1 neurons [Ohiorhenuan *et. al.*, Nature 466, (2010): 617], we quantitatively rule out the scenario that common inhibition causes the observed sparse activity characterized by negative triple-wise interactions among the neurons. Instead, we show that an alternative architecture with common excitatory inputs to pairs of neurons well explains it. The proposed analytical approach that connects neural mechanisms with neural interactions could serve as a useful tool to probe network architecture, using recordings of population activity.

Significance Statement

Inference of the network architecture from neural data is a daunting task. Here, we introduce a quantitative method that lets us reveal the underlying architecture. Using an exact analytic solution for input-output relation of a neuron model, we developed a mathematical framework that connects biophysical properties of individual neurons with neural population activity. With this method, we quantitatively compare two possible architectures in a particular experiment and rule out one hence suggest the other as the possible neuronal architecture for sparse population activity observed in visual neurons. This unified framework allows us to explore biophysical mechanisms of neural information processing from their population activity.

Introduction

One interest in neuroscience is to *reveal neural circuitries* using recorded neurons' activities that are constrained by synaptic connections, and the *nonlinear spiking dynamics* of individual neurons. There exist many theoretical studies, all trying to make a connection between *network structure* and *neural activity's statistics* (Hu et al., 2013, 2014; Ocker et al., 2017a; Ostojic et al., 2009; Pernice et al., 2011; Rosenbaum et al., 2017; Trousdale et al., 2012). However, nearly most of them consider a linear response around stationary distribution and did not take account of the nonlinearity in the single neuron's input-output relation(but see Ocker et al. 2017b). Such attempts are justified as long as synaptic strengths are weak enough so one single input is quite unlikely to cause the spike of the postsynaptic neuron; however such an assumption of weak synaptic input is in contrast with the task of revealing network architecture, where we cannot neglect strong synaptic connections.

Here we look at the simplest possible scenario, where the experimentalist records spiking activity of three neurons in vivo, but he/she cannot reveal neural connectivity directly. Will the three neurons spike independently, or be correlated due to shared inputs? In the latter case, are such inputs shared between each pair of them, or among three of them? Are shared inputs excitatory or inhibitory? And finally, does either of the three observed neurons make a direct synaptic connection to another of them? It is quite interesting that a closed-form analytic relation that addresses the nonlinearity of input-output in a spiking neuron model, lets us answer almost all of these questions.

By using the analytical model, we examine correlations in simultaneous spiking activity of two and three neurons in a small time window. For this aim, we use the information geometric measures of neural interactions (Nakahara and Amari, 2002), known as pairwise and

triple-wise interactions, that explain excess or paucity of synchronous spikes expected from their independent activity. The interaction among three neurons was experimentally examined by Ohiorhenuan et al. in V1 of monkey in vivo. They found significant negative triple-wise interactions if neurons are spatially close (Ohiorhenuan et al., 2010; Ohiorhenuan and Victor, 2011); it indicates significantly higher probability for simultaneous silence of three neurons. Hence the population activity is less synchronous compared to the activity without the triple-wise interactions, despite they exhibit positive pairwise correlations. The same negative triple-wise interactions were reported for nearby neurons in hippocampal slices (Shimazaki et al., 2015).

Recently, we theoretically investigated the statistical dependency of postsynaptic spikes on synaptic inputs for an LIF neuron, which includes synaptic and membrane dynamics (Shomali et al., 2018). Despite the fact that integration and thresholding mechanism of neuronal firing tend to regularize inter-spike intervals, neuronal spikes in vivo are highly variable (Shadlen and Newsome, 1998; Softky and Koch, 1993); it is suggested to be the result of balanced inputs from excitatory and inhibitory neurons near spiking threshold (Shadlen and Newsome, 1998; Vreeswijk and Sompolinsky, 1996, 1998). We derived the dependency of output spikes on the synaptic input of interest, called a signaling input, in a noisy background, when the membrane potential is close to the threshold regime (Shomali et al., 2018), a condition neuron encounters in vivo during stimulus presentation (Tan et al., 2014). The resultant exact analytical solution of the spike timing density serves as a useful method to study neural population activity in more realistic conditions than previous studies.

Here, using the established relationship between the signaling input and spikes of postsynaptic neurons, we elucidate the impact of common signaling input on the population activity. More specifically, we construct a unified model that connects the synaptic inputs, spiking nonlinearity, network architecture with different types of common inputs, and statistics of population activity for a small number of neurons. Next, based on this theoretical study, we reveal possible architecture behind the observed sparse population activity characterized by the negative triple-wise interactions (Ohiorhenuan et al., 2010).

Materials and Methods

Leaky integrate-and-fire neuron at the threshold regime

In this subsection, we briefly introduce the exact statistical solution of the postsynaptic spike density (Shomali et al., 2018). The neuron receives a synaptic input (a signaling input) on top of background weak synaptic inputs that bring the membrane potential close to the threshold. The background activity is modeled as the Gaussian white noise which may replicate the synaptic inputs to V1 neurons when a visual stimulus is presented (Tan et al., 2014). Below, we bring the stochastic differential equation for membrane potential of the LIF neuron model, and the solution for the Inter-Spike-Interval (ISI) density when neuron receives the signaling input on top of the Gaussian noise.

We consider an LIF neuron with membrane time constant of τ_{m} and threshold voltage of V_θ, receiving transient signaling input, ΔI, at time τ_b, and independent Gaussian noise, I_0 (Fig 1A):

$$\tau_{\mathrm{m}}\frac{dV}{dt} = -(V - V_r) + I(t), \tag{1}$$

the input current, $I(t)$ is:

$$I(t) = I_0(t) + \Delta I(t, \tau_b), \tag{2}$$

where $I_0(t)$ is the background input induced by presynaptic neurons and $\Delta I(t, \tau_b)$ is the transient signaling input. The background input has a mean ($\bar{I}$) and a variance ($2D/\tau_{\mathrm{m}}$) where D is the diffusion coefficient.

The ISI density as a function of signaling input's amplitude (A) and spike timing (τ_b) for arbitrary shape of transient signaling input (ΔI) when $t \geq \tau_b$ at the threshold regime, reads (Shomali et al., 2018):

$$\begin{aligned} J(V_\theta, t) = \frac{\sqrt{\kappa\omega}}{\pi\tau_{\mathrm{m}}}\{ \exp(-\frac{\varphi_+^2}{2})[1 + \sqrt{\frac{\pi}{2\kappa}}\varphi_+ \exp(\frac{\varphi_+^2}{2\kappa}) \times (1 + Erf(\frac{\varphi_+}{\sqrt{2\kappa}}))] - \\ \exp(-\frac{\varphi_-^2}{2})[1 + \sqrt{\frac{\pi}{2\kappa}}\varphi_- \exp(\frac{\varphi_-^2}{2\kappa}) \times (1 + Erf(\frac{\varphi_-}{\sqrt{2\kappa}}))]\}, \end{aligned} \tag{3}$$

where $Erf(x) = (2/\sqrt{\pi}) \int_0^x \exp(-t^2)dt$, $r(t) = \exp(-t/\tau_{\mathrm{m}})$ and $\kappa(t, \tau_b)$, $\omega(t, \tau_b)$ and $\varphi_\pm(t, \tau_b)$ are:

$$\begin{aligned} \kappa(t, \tau_b) &= (1 - r(t)^2)/(1 - r(t - \tau_b)^2), \\ \omega(t, \tau_b) &= \frac{r(t - \tau_b)^2(1 - r(\tau_b)^2)}{(1 - r(t)^2)^3}, \\ \varphi_\pm(t, \tau_b) &= \sqrt{\frac{\tau_{\mathrm{m}} V_\theta^2}{D(1 - r(\tau_b)^2)}}\{ \pm r(\tau_b) - \int_{\tau_b}^{t} \frac{ds}{\tau_{\mathrm{m}}} \frac{\Delta I(s, \tau_b)}{V_\theta}\}. \end{aligned} \tag{4}$$

In the absence of signaling input ($t < \tau_b$), the ISI density reduces to the known formula (Tuckwell, 1988; Wang and Uhlenbeck, 1945):

$$J_0(V_\theta, t) = \frac{1}{\tau_{\mathrm{m}}} \sqrt{\frac{2}{\pi} \frac{\tau_{\mathrm{m}} V_\theta^2}{D} \frac{r^2(t)}{(1 - r^2(t))^3}} \exp[-\frac{\tau_{\mathrm{m}} {V_\theta}^2}{2D} \frac{r^2(t)}{1 - r^2(t)}]. \tag{5}$$

In the following analysis, we use Eq 3 with a square shape of signaling input given by

$$\Delta I(t, \tau_b) = A \times \begin{cases} 0 & t < \tau_b, \\ 1/\Delta t & \tau_b \leq t \leq \tau_b + \Delta t, \\ 0 & \tau_b + \Delta t < t, \end{cases} \tag{6}$$

Spiking density of LIF neuron after signaling input arrival

In order to further analyze the effect of the signaling input, it is convenient to consider postsynaptic spike timing relative to the arrival time of the signaling input (Fig 1A, Left). We reset the time origin to the timing of signaling input arrival, and find the density $f(\tau)$ that postsynaptic neuron spikes at τ after the signaling input arrival. Suppose that the last spike of the postsynaptic neuron occurred at τ_b ms before the arrival of signaling input (Fig 1A, Right).

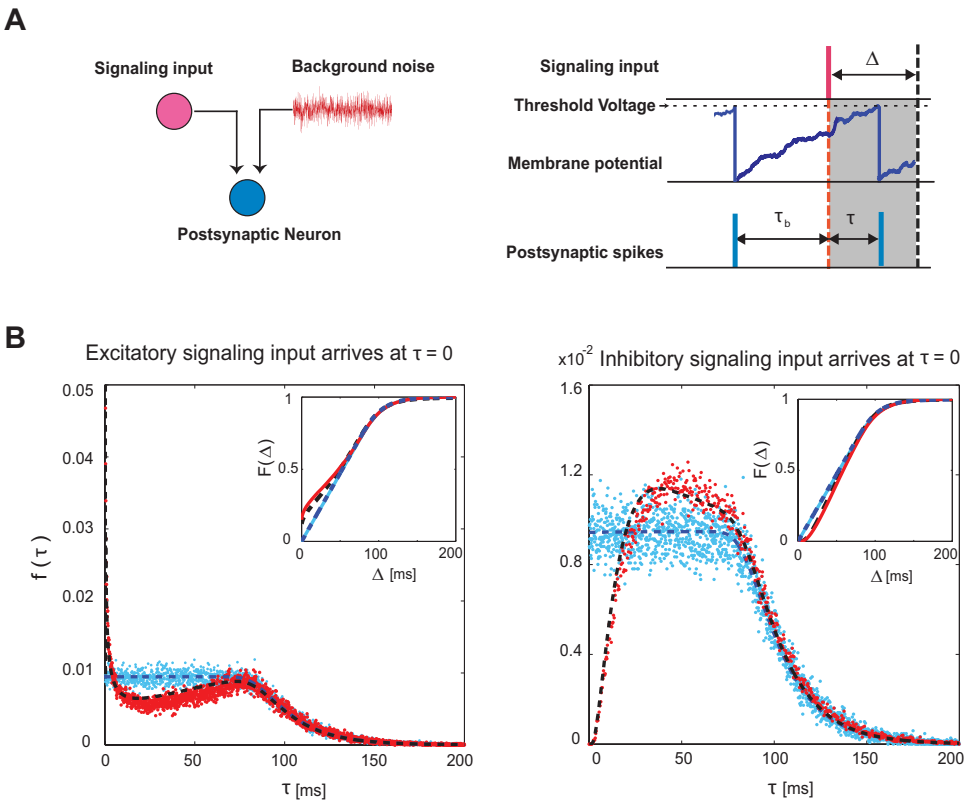

Fig 1. Analysis of a postsynaptic neuron receiving signaling input on top of the background noise. (**A**) Left: A schematic model of postsynaptic neuron driven by background Gaussian noise and a transient signaling input. Right: Timing of postsynaptic spikes and the arrival time of signaling input. Postsynaptic neuron generates spike (blue tick) and resets, signaling input(red tick) arrives at τ_b after last spike of postsynaptic neuron; it changes the voltage trajectory of membrane potential upon arrival. The postsynaptic spike occurs at τ after arrival time of the signaling input. The gray shaded area of width Δ indicates the observation time window during which the probability of postsynaptic activity pattern is computed. (**B**) The probability density of the first spike at time τ after arrival (Eq 8) of excitatory (left) and inhibitory (right) signaling input. The simulation results (red dots) and the analytical solutions (dashed black line, Eq 8) are well matched. The same results for signaling input with zero amplitude are depicted; the analytic (dashed blue line) and simulation results (blue dots) well coincide. Inset: The probability of spiking during Δ (CDF) after signaling input arrival (Eq 9). The parameters are: $V_\theta = 20mV$, $\tau_m = 20ms$, $A = 5mV\ ms$, and the diffusion coefficient is $D = 0.74(mV)^2ms$. The values of the parameters are chosen using the physiologically plausible range (McCormick et al., 1985).

Then the conditional density of postsynaptic spike time, $f(\tau|\tau_b)$, is calculated as (Shomali et al.,

2018):

$$f(\tau|\tau_b) = \frac{J(V_\theta, \tau + \tau_b)}{1 - \int_0^{\tau_b} J(V_\theta, s)ds}, \tag{7}$$

where the denominator is a normalization term to satisfy $\int_0^\infty f(\tau|\tau_b)d\tau = 1$.

Next, we compute the probability density of the postsynaptic spike timing averaged over various timings of τ_b. Given the fixed time origin at the signaling input arrival, the probability density of the duration τ_b is known to follow the probability of backward recurrence time from the renewal point process theory (Cox, 1962). This density is given as $p(\tau_b) = \mu[1 - \int_0^{\tau_b} J_0(V_\theta, s)\, ds]$, where μ is the mean firing rate of postsynaptic neuron when there is no signaling input, given as $\mu = (\int_0^\infty sJ_0(V_\theta, s)\, ds)^{-1}$. By marginalizing Eq 7 with respect to τ_b and using the backward recurrence time, $p(\tau_b)$, we obtain (Shomali et al., 2018):

$$\begin{aligned} f(\tau) &= \int_0^\infty f(\tau|\tau_b)p(\tau_b)\, d\tau_b \\ &= \int_0^\infty \mu J(V_\theta, \tau + \tau_b)\, d\tau_b. \end{aligned} \tag{8}$$

Note that when the amplitude of signaling input, A, is diminished to zero, $J(V_\theta, t) = J_0(V_\theta, t)$ and $f(\tau)$ simplifies to $f_0(\tau) = \int_\tau^\infty \mu J_0(V_\theta, s)\, ds$.

The probability of having one or more spike events in time window Δ is given by a cumulative density function of $f(\tau)$:

$$F_A(\Delta) = \int_0^\Delta f(\tau)d\tau, \tag{9}$$

where the subscript A indicates that it is the function of amplitude of the signaling input. In the absence of signaling input, we have $F_0(\Delta) = \int_0^\Delta f_0(\tau)d\tau$. Based on the probability of spiking within specific window Δ, $F_A(\Delta)$, one can find the probability of patterns considering the assumption that neurons are conditionally independent. This calculation is described in the next section.

Figure 1B shows the marginalized spiking density at time τ after signaling input arrival for squared shape input (Eq 6, dashed black lines). Early spiking (small τ) after the arrival of excitatory (inhibitory) input is highly more (less) probable, compared to no-signaling input case (dashed blue lines). However, the spiking densities with or without the signaling input are virtually identical at sufficiently large τ; indicating the short-lasting effect of the signaling input. Accordingly, the cumulative distribution functions, $F_A(\Delta)$, (Fig 1 insets) with or without the signaling input differ for small Δ, but are indistinguishable for large Δ. This result implies that we cannot discern the presence of signaling input if we use large time window.

Results

Neural interactions as a function of signaling input and network architecture

In this section, we connect the single neuron properties to statistics of population activity. For this goal, we analyze correlated activity of a small number of neurons when they receive

common signaling inputs. To formally investigate the neuronal interactions including higher-order interactions, we use the information geometric measure of correlations (Amari, 2009b; Martignon et al., 2000; Nakahara and Amari, 2002). The higher-order interaction measured by this framework indicates the neuronal interactions that cannot be expected by the lower order statistics.

I. Pairwise interaction in the presence of a common signaling input

We analyze the interaction of two postsynaptic neurons receiving a common signaling input in addition to independent background noise (Fig 2A, Top). The middle panel of Fig 2A illustrates the timing of postsynaptic spikes before and after the common input arrival. By binning their spike sequences with a Δ time window (Fig 2A, Middle, and Left), we compute probabilities of activity patterns of postsynaptic neurons. We assume that neurons sparsely receive a random common input with firing rate λ in a Poissonian fashion. We then, segment the spike sequences using bins aligned at the onset of common input. Let $x_i = \{0, 1\}$ $(i = 1, 2)$ be a binary variable, where $x_i = 1$ represents that the ith neuron emitted one or more spikes in the bin, and $x_i = 0$ represents that the neuron was silent.

We denote by $P(x_1, x_2)$ the probability mass function of the binary activity patterns of the two postsynaptic neurons. Here $P(1, 1)$ and $P(0, 0)$ are the probabilities that both neurons are, respectively, active and silent within Δ. Similarly, $P(1, 0)$ is the probability that neuron 1 emits one or more spikes while neuron 2 is silent during Δ; $P(0, 1)$ represents the opposite situation. The probability mass function is represented in the form of an exponential family distribution as

$$P(x_1, x_2) = \exp\left(\theta_1^{\mathrm{p}} x_1 + \theta_2^{\mathrm{p}} x_2 + \theta_{12}^{\mathrm{p}} x_1 x_2 - \psi\right), \tag{10}$$

where $(\theta_1^{\mathrm{p}}, \theta_2^{\mathrm{p}}, \theta_{12}^{\mathrm{p}})$ are the canonical parameters, and ψ is a log-normalization parameter. In particular, θ_{12}^{p} is an information geometric measure of pairwise interaction (Amari, 2001, 2009b; Nakahara and Amari, 2002). Accordingly, pairwise interaction parameter is computed as:

$$\theta_{12}^{\mathrm{p}} = \log \frac{P(1, 1)P(0, 0)}{P(1, 0)P(0, 1)}. \tag{11}$$

If the binary activity of two neurons are independent, then $\theta_{12}^{\mathrm{p}} = 0$.

For two neurons, we construct the probabilities of the activity patterns by using the probability of spike occurrence in a bin Δ (Eq 9). Since two neurons receive common inputs, they are conditionally independent. Thus using Eq 9:

$$P_A(x_1, x_2) = P_A(x_1)P_A(x_2) = \prod_{i=1}^{2} F_A(\Delta)^{x_i}(1 - F_A(\Delta))^{1-x_i}, \tag{12}$$

where A stands for the amplitude of common input current. So $A = 0$ represents the absence of common input. Since the rate of common input is λ, it is applied at $\lambda\Delta \times 100\%$ of the bins whereas it is absent in $(1-\lambda\Delta) \times 100\%$ of the bins. Accordingly, we consider the spike sequences of two postsynaptic neurons as a mixture of the two conditions, with or without the common input. Hence the probabilities of the activity patterns would be:

$$P_{\mathrm{mix}}(x_1, x_2) = (\lambda\Delta)P_A(x_1, x_2) + (1 - \lambda\Delta)P_0(x_1, x_2). \tag{13}$$

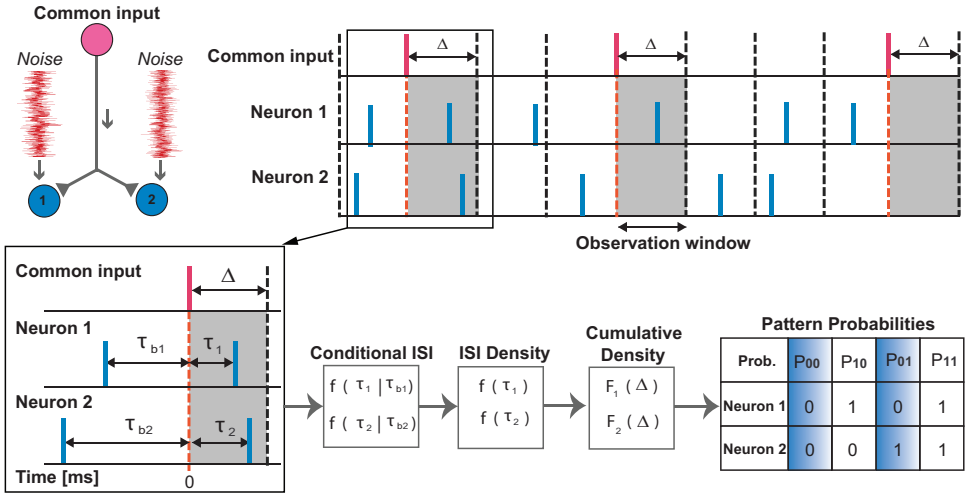

Fig 2. Analysis of two neurons receiving common signaling input on top of background noise. Top, left: A schematic model of two postsynaptic neurons (Neuron 1 and Neuron 2, blue circles) driven by independent noise and a common signaling input (pink circle). Top, right: Spike trains of two postsynaptic neurons (blue spikes) receiving common signaling inputs (red spikes) with rate λ. The gray shaded area of width Δ indicates the observation time window during which we compute the probabilities of postsynaptic activity patterns. Bottom, left: Timing of postsynaptic spikes relative to the arrival time of the common input. The last spike of Neuron 1 (Neuron 2) has occurred τ_{b1} (τ_{b2}) before the arrival of common input, and their next spikes happen at τ_1 (τ_2) after that. Bottom, middle: The conditional ISI density after input arrival is calculated by Eq 7. Marginalizing over previous spike (τ_b), the probability of spiking after input arrival (ISI density) is achieved (Eq 8). The next step is calculating the cumulative density function (Eq 9) that is the probability of having one or more spikes within window Δ. Bottom, right: Based on $F_A(\Delta)$ and the fact that neurons are independent, the probability of having a particular pattern of spikes for two neurons is obtained. Four possible binary activity patterns $(00, 01, 10, 11)$ of two postsynaptic neurons and their associated probabilities (P_{ij}, $i, j \in \{0, 1\}$). The '1' denotes occurrence of at least one spike within the Δ time window, whereas the '0' represents the silence of neuron within this window.

The pairwise interaction predicted by the mixture model is compared with simulated spike sequences (Eq 11, 13). Figure 3A displays the interaction for different bin sizes, Δ, when the two neurons receive common excitatory input. The pairwise interaction predicted by the mixture model agrees with the simulation results (Left panel, red and gray lines respectively). θ^{p}_{12} has an increasing trend with the rate of common input (Fig 3A, Right). However, if we increase the bin size, the probability of having one or more spikes within Δ increases and saturates to 1 (Fig 2B, Inset) regardless of presence or absence of the signaling input. It means $F_A(\Delta)/F_0(\Delta) \to 1$, which results in vanishing pairwise interaction as the bin size increases. In sum, we can hardly discriminate between the presence and absence of common input if we use a large bin size.

We examine pairwise interactions by changing two independent parameters, scaled amplitude

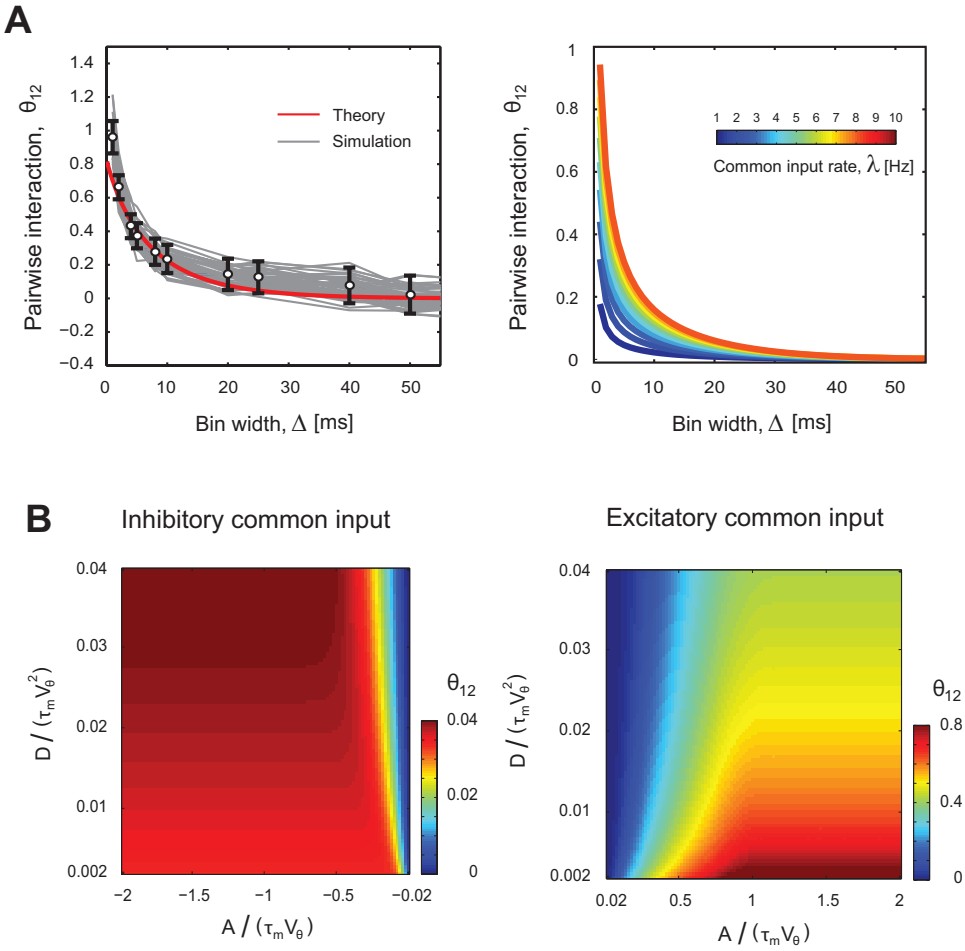

Fig 3. Analysis of the interaction between two neurons receiving common signaling input on top of background noise. (**A**) Interaction of two postsynaptic neurons (θ_{12}^{p}, Eq 11) as a function of bin size, Δ. The parameters are: $\tau_m = 20ms$, $V_\theta = 20mV$, $A = 5mV\ ms$ and $D = 0.74(mV)^2ms$. Left: The pairwise interaction computed from simulated spike sequences (gray lines: 50 individual trials each containing about 2500 spike occurrence of common input; dots and error bars: mean$\pm$standard deviation) and the analytic result of the mixture model (red line, Eq 11) for common input rate $\lambda = 5Hz$. Right: Analytical value of θ_{12}^{p} as a function of Δ for different common input rates, λ. (**B**) The pairwise interaction as a function of two scaled parameters, $D/(\tau_m V_\theta^2)$ and $A/(\tau_m V_\theta)$ for excitatory (right) and inhibitory (left) common inputs with $\lambda = 5Hz$ and $\Delta = 5ms$.

of the signaling input $A/(\tau_m V_\theta)$ and scaled variability of the noisy background input $D/(\tau_m V_\theta^2)$ (Fig 3B). As expected, the pairwise interactions are positive for both common excitatory and inhibitory inputs. However, the interactions are significantly weaker in the inhibitory case. It implies that it is difficult to observe the effect of inhibitory common input for this range of

postsynaptic firing rate and that the strong pairwise interactions are the indicator of having common excitatory input.

For each value of normalized diffusion coefficient, $D/(\tau_m V_\theta^2)$, there exists a critical normalized amplitude for common excitatory input, $A/(\tau_m V_\theta) \sim 1$. From that critical value on, postsynaptic neuron's spiking density, and consequently pairwise interaction, does not change anymore (Fig 3B, Right). The saturation value of pairwise interaction is inversely correlated with normalized diffusion coefficient; since higher normalized diffusion coefficient disperses the voltage trajectories of membrane potential, the probability of spiking after common input arrival decreases. Similar behavior for θ_{12}^{p} is observed for inhibitory input (Fig 3B, Left). Nevertheless, in contrary to the common excitatory input case, pairwise interaction and $D/(\tau_m V_\theta^2)$ are directly correlated.

II. Higher-order interaction among three neurons receiving common signaling inputs

We now extend the analysis of neural interactions to three neurons. In the exponential form, the probability mass function of binary activity patterns for three neurons is written as

$$P(x_1, x_2, x_3) = \exp\left(\sum_{i=1}^{3} \theta_i^{\mathrm{t}} x_1 + \sum_{i<j} \theta_{ij}^{\mathrm{t}} x_i x_j + \theta_{123}^{\mathrm{t}} x_1 x_2 x_3 - \psi\right). \tag{14}$$

If $\theta_{123}^{\mathrm{t}}$ (the triple-wise interaction parameter) is 0, the distribution reduces to the pairwise maximum entropy model, i.e., the least structured model that maximizes the entropy given that the event rates of individual neurons and joint event rates of two neurons are specified (Cover and Thomas, 1991). That is, a positive (negative) triple-wise interaction indicates that the three neurons generate synchronous events more often (less) than the chance coincidence expected from event rates of individual neurons and their pairwise correlations. From this equation, the triple-wise interaction among three neurons for exponential family of probability mass function, is calculated as (Amari, 2009a; Nakahara and Amari, 2002):

$$\theta_{123}^{\mathrm{t}} = \log \frac{P(1,1,1)P(1,0,0)P(0,1,0)P(0,0,1)}{P(0,0,0)P(0,1,1)P(1,0,1)P(1,1,0)}. \tag{15}$$

Here, studying interaction among three neurons is motivated by some experimental studies (Ohiorhenuan et al., 2010; Ohiorhenuan and Victor, 2011) which recorded the activity of three neurons simultaneously. Two possible scenarios during recording of three neurons can happen for common input (Fig 4A); common input can be shared among three neurons (red connections) or it can be shared between two neurons (green connections). Assuming symmetry, the former one leads to star architecture (Fig 4B, left) while the latter one makes the triangle architecture (Fig 4B, right). So in the following, we investigate triple-wise interactions of neurons under two different architectures of the common signaling input.

In the first architecture (star architecture), three neurons receive a single common signaling input at the same time (Fig 4B, Left). The conditional probability of activity patterns given a common input to all three neurons is $P_A(\mathbf{x}) = \prod_{i=1}^{3} F_A(\Delta)^{x_i}(1 - F_A(\Delta))^{1-x_i}$. Similarly, the probability mass function of three neurons without any common input is obtained as

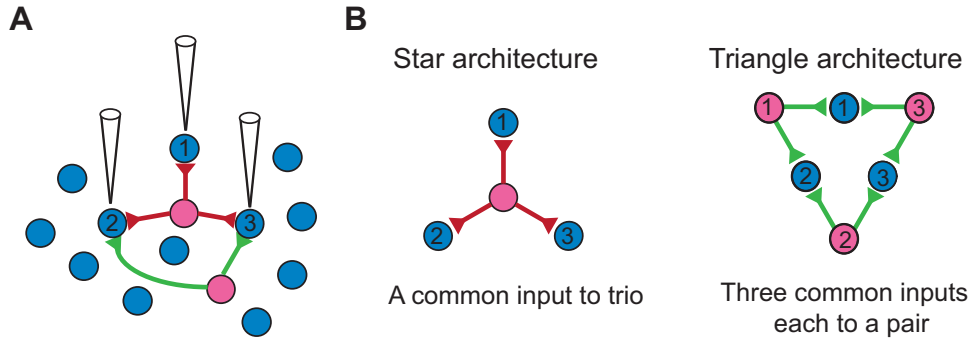

Fig 4. The activity of three postsynaptic neurons are recorded simultaneously. (**A**) The neurons (blue circles) would act independently in the absence of any *common input*. A common input (pink circle) could be an input to three of them (red connections), or at least two of them (green connections). This leads to two major family of underlying architectures and thus behaviors: the *star architecture* which addresses a common input to the three postsynaptic neurons (**B**, left), and the triangle architecture that common inputs are given to each pair of three postsynaptic neurons (**B**, right). We have further symmetry among them so that a common input to one pair is accompanied by two other common inputs to the two other pairs.

$P_0(\mathbf{x}) = \prod_{i=1}^{3} F_0(\Delta)^{x_i}(1 - F_0(\Delta))^{1-x_i}$. Thus, we model spike occurrence by a mixture of the two conditions, with or without common input, as:

$$P(\mathbf{x}) = \lambda\Delta P_A(\mathbf{x}) + (1 - \lambda\Delta)P_0(\mathbf{x}). \tag{16}$$

In the second architecture (triangular architecture), each pair of three neurons receives common signaling input from an independent presynaptic neuron with frequency λ (Fig 4B, Right). The first, second, and third common inputs project to neuron 1 and 2, neuron 2 and 3, and neuron 1 and 3, respectively. The three common inputs are independent from each other, and happen with an equal frequency, λ. When the first common input is active but the two other common inputs are silent, the pattern probabilities of three postsynaptic neurons are given as $P_A^1(\mathbf{x}) = [\prod_{i=1}^{2} F_A(\Delta)^{x_i}(1 - F_A(\Delta))^{1-x_i}] \times [F_0(\Delta)^{x_3}(1 - F_0(\Delta))^{1-x_3}]$. This situation happens in $(\lambda\Delta)(1 - \lambda\Delta)^2 \times 100\%$ of the bins. The probabilities of activity patterns at which neurons receive from the second (third) common input, $P_A^2(\mathbf{x})$ ($P_A^3(\mathbf{x})$), are given similarly to this equation. Here we note that the common inputs may be simultaneously applied at the same bin because of their independence. Namely, two common inputs coincide at $(\lambda\Delta)^2(1 - \lambda\Delta) \times 100\%$ of the bins. The pattern probability in the bins at which common inputs 1 and 2 coincide is given by $P_A^{12}(\mathbf{x}) = [\prod_{i=1,3} F_A(\Delta)^{x_i}(1 - F_A(\Delta))^{1-x_i}] \times [F_{2A}(\Delta)^{x_2}(1 - F_{2A}(\Delta))^{1-x_2}]$. Similarly, we define $P_A^{23}(\mathbf{x})$ and $P_A^{13}(\mathbf{x})$ for the bins at which the common inputs 2 and 3, and the common inputs 1 and 3 coincide, respectively. Finally, all common inputs coincide at $(\lambda\Delta)^3 \times 100\%$ of the bins, at which the pattern probability is given by $P_A^{123}(\mathbf{x}) = \prod_{i=1,2,3} F_{2A}(\Delta)^{x_i}(1 - F_{2A}(\Delta))^{1-x_i}$. Thus,

the parallel spike sequences are modeled as a mixture of these probability mass functions,

$$P(\mathbf{x}) = (1-\lambda\Delta)^3 P_0(\mathbf{x}) + \sum_{i=1}^{3}(\lambda\Delta)(1-\lambda\Delta)^2 P_A^i(\mathbf{x}) + \sum_{i<j}(\lambda\Delta)^2(1-\lambda\Delta)P_A^{ij}(\mathbf{x}) + (\lambda\Delta)^3 P_{2A}^{123}(\mathbf{x}). \tag{17}$$

The triple-wise interaction parameters computed from simulated spike sequences of postsynaptic neurons are compared with the theoretical predictions, using the mixture models (Fig 5A and B, Left). Activities of neurons that receive a simultaneous common excitatory input (star architecture) are characterized by positive triple-wise interactions (Fig 5A, Left) whereas activities of neurons that receive independent common excitatory inputs to pairs (triangular architecture) are characterized by negative triple-wise interactions (Fig 5B Left). Figure 5A and B, Right, show a decreasing trend for triple-wise interaction as the bin size increases; by the same reason given for pairwise interaction (Fig 3A, Right). The dependency of the triple-wise interaction on the common input rate is also shown in right panels in Fig 5A and B.

Figure 5C shows triple-wise interactions under star (Top) and triangular (Bottom) architectures for excitatory (Right) and inhibitory (Left) common input as a function of scaled diffusion coefficient $D/(\tau_m V_\theta^2)$ and scaled amplitude $A/(\tau_m V_\theta)$. A single common excitatory input, in the star architecture, significantly increases the probability that all three neurons spike in the observation time window of Δ, $P(1,1,1)$; whereas a single common inhibitory input increases the probability of the reverse pattern, $P(0,0,0)$. This simply changes the sign of $\theta_{123}^{\mathrm{t}}$ in Eq 15. In the triangular architecture, with common excitatory input, however, each common input causes postsynaptic spike for two neurons and does not drive the other one. This primarily increases $P(1,1,0)$ (or any other of its permutations) and attenuate the fraction (Eq 15); it means negative $\theta_{123}^{\mathrm{t}}$. For common inhibitory input, the probability of the reversed pattern, $P(0,0,1)$ (or any other permutations) increases; this results in larger nominator in Eq 15 and positive triple-wise interaction. These results demonstrate that not only the type of common input (excitation or inhibition) but also the underlying architecture (star or triangular) determines the sign of triple-wise interactions. This helps us to relate the ubiquitously observed negative triple-wise interaction in activities of cortical neurons (Ohiorhenuan et al., 2010; Ohiorhenuan and Victor, 2011; Shimazaki et al., 2012; Yu et al., 2011) to either star architecture with inhibitory input or triangular structure with excitatory input. Notably, in both architectures, the triple-wise interactions for the common inhibitory inputs are significantly weaker, *i.e.* harder to measure experimentally, than those expected for common excitatory inputs.

Network structure and common input type explain neural activity in vivo; comparison with experimental data

Above observations raise a question; whether we can select the type of common input and underlying architecture that can explain the event activity of neuronal population. Figure 6 shows the first-order, pairwise and triple-wise interactions of 3 neurons in star or triangular architecture, receiving either common excitatory or inhibitory inputs. The interactions are calculated for some different values of scaled amplitude of common input ($A/(\tau_m V_\theta)$) and diffusion coefficient

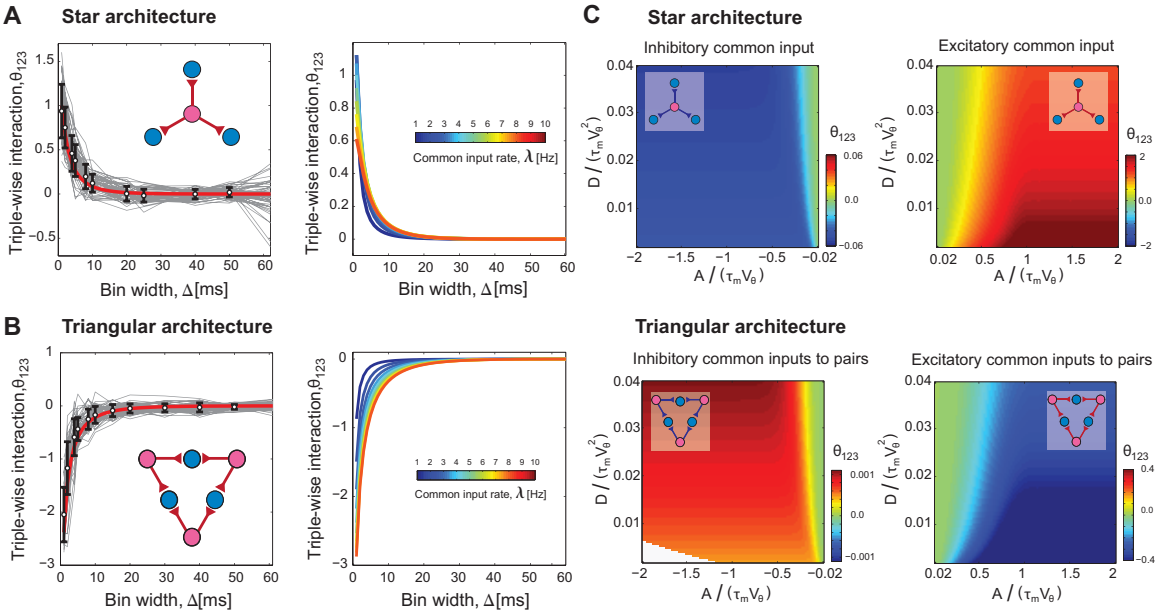

Fig 5. Triple-wise interaction of 3 LIF neurons in two architectures, receiving common inputs on top of independent noise. (**A**) The interaction when the postsynaptic neurons, blue ones, are in a star architecture receiving a single excitatory $A = 5mV\ ms$ common input at the same time. The parameters are: $\tau = 20ms$, $V_\theta = 20mV$, $A = 5mV\ ms$ and $D = 0.74(mV)^2ms$. **Left**: The triple-wise interaction computed from simulated spike sequences (gray lines: 50 individual trials each containing about 2500 spike occurrence of common input; dots and error bars: mean$\pm$standard deviation) and the analytic result of the mixture model (red line, Eq 15) for $\lambda = 5Hz$. **Right**: Analytical value of $\theta^{\mathrm{t}}_{123}$ as a function of Δ for different common input rates, λ. (**B**) The triple-wise interaction when the postsynaptic neurons, blue ones, are in a triangular architecture. Each pair of postsynaptic neurons receives an independent common excitatory input. The parameters are as in (A). **Left**: The triple-wise interaction as a function of Δ. **Right**: Analytical value of $\theta^{\mathrm{t}}_{123}$ as a function of Δ for different common input rates, λ. (**C**) Triple-wise interactions of 3 neurons receiving common excitatory or inhibitory inputs under star (Top panel) and triangular (Bottom panel) architectures. $\theta^{\mathrm{t}}_{123}$ is represented as a function of two scaled parameters: $D/(\tau_m V_\theta^2)$ and $A/(\tau_m V_\theta)$, while other parameters are: $\lambda = 5Hz$ and $\Delta = 5ms$. White color in bottom left panel shows numerically indeterminate region due to very small diffusion coefficient and strong inhibition. The right-hand side figures are for excitatory and the left-hand side ones are for common inhibitory inputs.

$(D/(\tau_m V_\theta^2))$ which cover the physiologically plausible range. Figure 6A shows that the same θ^{t}_1 may be realized by different combinations of $A/(\tau_m V_\theta)$ and $D/(\tau_m V_\theta^2)$ for two architectures and common input type; thus it would be impossible to identify the underlying architecture and the type of common input only from the first-order parameter.

Nevertheless, we found that the four combinatorial cases occupy distinct regions in the θ^{t}_{12} versus $\theta^{\mathrm{t}}_{123}$ plane (Fig 6B). Thus, in principle, by investigating the interaction parameters, it is

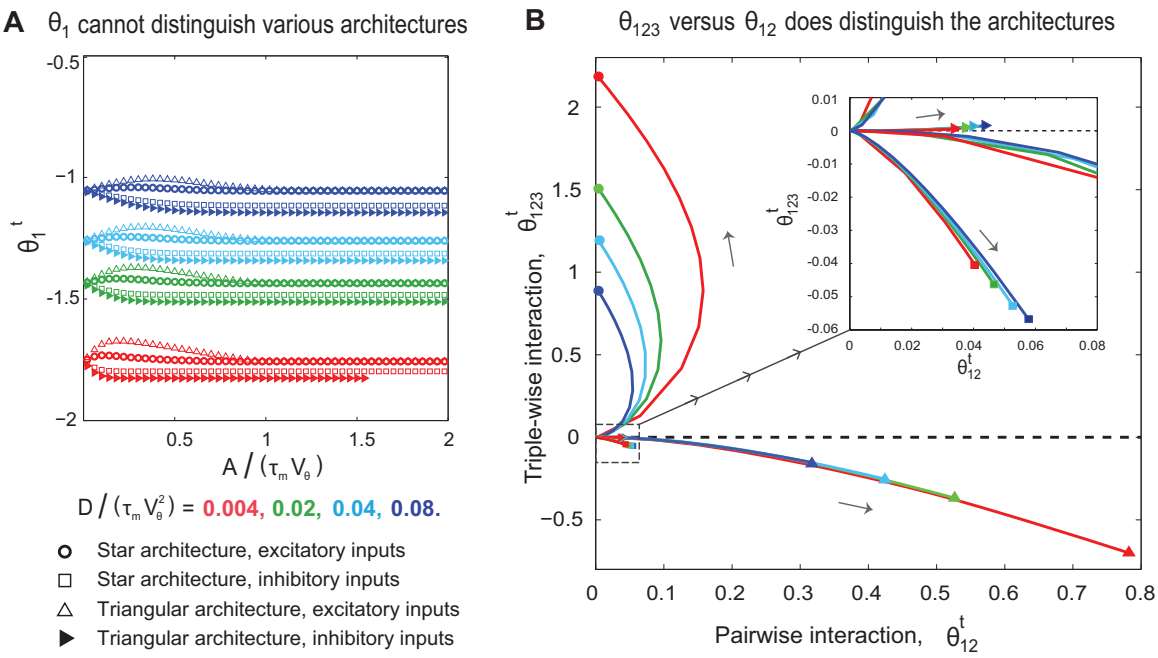

Fig 6. Natural parameters among population activity of 3 LIF neurons receiving common inputs in star and triangular architectures. (**A**) The natural parameter for individual neurons, θ_1^{t}, in star and triangular architectures with common excitatory or inhibitory inputs (four cases are shown by four symbols in the bottom) as a function of $A/(\tau_m V_\theta)$. The color code represents four different scaled diffusion coefficients, $D/(\tau_m V_\theta^2)$. (**B**) The triple-wise interaction versus pairwise interaction for star and triangular architectures with common excitatory and inhibitory inputs. The symbols and the color code are as in (A). The arrows indicate the increasing direction of the scaled amplitude parameter (i.e. $A/(\tau_m V_\theta)$) and the filled symbols show the saturation points. The inset illustrates the interactions in the neighborhood of origin. Comparing (A) and (B), it is clear that θ_1^{t} can hardly be used to distinguish between star and triangular architectures, whereas the two dimensional map of $\theta_{123}^{\mathrm{t}}$ versus θ_{12}^{t} can distinctly separate different architectures and even the type of common inputs especially when the interactions are not very weak. Fixed parameters are $\Delta = 5ms$ and $\lambda = 5Hz$.

possible to identify the underlying architecture and the type of common inputs (excitation or inhibition) to three homogeneous LIF neurons. However, within each of the conditions (except for star architecture with common excitatory inputs), the parameters overlap, which makes it impossible to identify the underlying parameters such as the input's amplitude or diffusion coefficient from the interaction parameters. Finally, both pairwise and triple-wise interactions are considerably weak when the neurons receive inhibitory inputs. It means, substantially sparser population activity due to the higher-order interaction can be generated if they are produced from common excitatory inputs under the triangular architecture, rather than common inhibitory inputs under the star architecture.

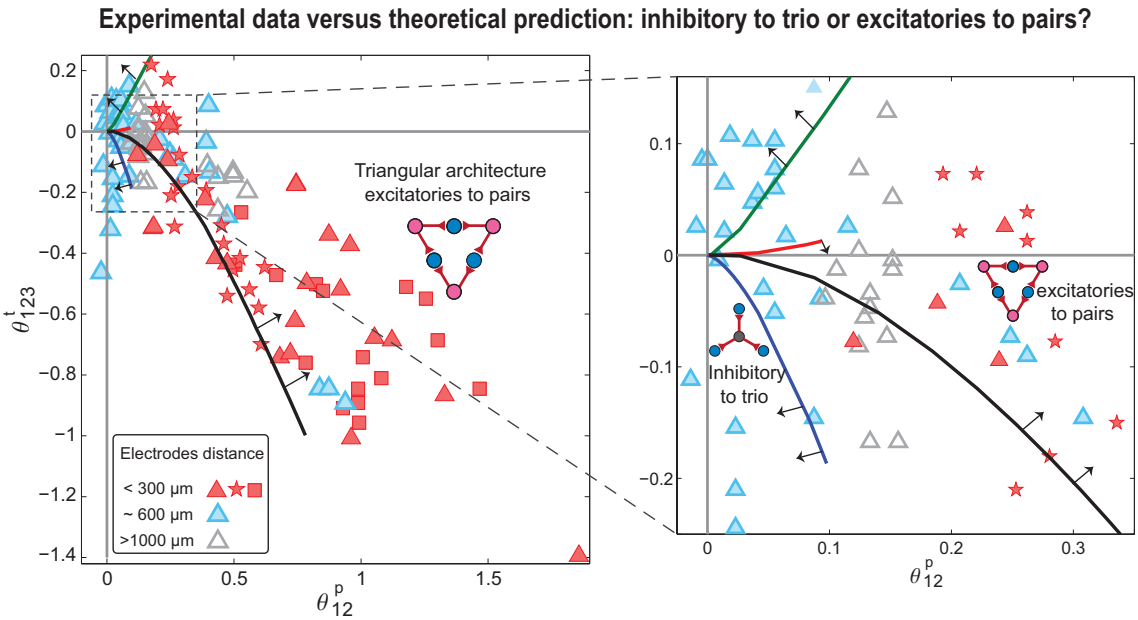

Fig 7. Comparison of theoretical predictions about neural interactions with experimental data extracted from (Ohiorhenuan and Victor 2011, Figure 4b). The data is recorded from V1 neurons of Macaque Monkeys using tetrodes. They analyzed the relation between triple-wise interaction (Eq 15) of three neurons (ordinate) and an average marginal pairwise interaction (Eq 11) of neuron pairs in the group (abscissa). Red and blue filled symbols represent interactions of neurons within 300 and $600\mu m$ vicinity respectively while unfilled grey symbol shows interaction of neurons at > 1000 microns distance. The dashed black line shows interactions theoretically obtained by assuming triangular architecture with common excitatory inputs, using a tiny value of $D/(\tau_m V_\theta^2) = 4 \times 10^{-8}$ for different $A/(\tau_m V_\theta)$. Similarly, the blue dashed line is the prediction for star architecture with common inhibitory inputs using the largest value $D/(\tau_m V_\theta^2) = 4$, that we could compute without numerical instability. The right panel magnifies near the origin of the left figure. Here the green (red) dashed line shows the lower (upper) boundaries for star architecture with common excitatory inputs (triangular architecture with common inhibitory inputs). Fixed parameters are $\Delta = 5ms$ and $\lambda = 5Hz$. The data reveals that nearby neurons (red filled symbols) receive pair of excitatory inputs in triangular architecture rather than inhibitory inputs in star architecture.

In Fig 7, we compare experimental data with our theoretical predictions. The previous study (Ohiorhenuan and Victor, 2011) investigated the relation between triple-wise interaction (Eq 15) of three neurons (ordinate) and an average marginal pairwise interactions (Eq 11) of neuron pairs in the group (abscissa). Their analysis showed that many of local neurons that are separated within 300 μm exhibited positive pairwise and negative triple-wise interactions. According to the analysis in the previous section, there are two alternative hypotheses to explain such interactions: common excitatory inputs with the triangular architecture or inhibitory

inputs with the star architecture. Between the two, we found that triangular architecture with common excitatory inputs can reproduce the empirical interactions. The dashed black line shows theoretical interactions, assuming the triangular architecture with common excitatory inputs, using a very small value of $D/(\tau_m V_\theta^2) = 4 \times 10^{-8}$ for different $A/(\tau_m V_\theta)$. Note that the interactions expected for larger and more physiologically plausible values of $D/(\tau_m V_\theta^2)$ occupy in-between this line and the abscissa. Thus, this architecture is likely to reproduce most of the empirical interactions found in neurons in a local circuitry. To the contrary, it is unlikely for star architecture with common inhibitory input to explain the strong negative interactions (see the blue dashed line; Note that interactions expected for smaller values of $D/(\tau_m V_\theta^2)$ occupy in-between this line and the ordinate).

Discussion

The aim of this study is to make a link between network architecture, statistics of neural activity and nonlinearity between input and output of the neurons. To connect network architecture with population activity, we firstly used the established conditional ISI density of LIF neurons receiving signaling input near the threshold regime (Shomali et al., 2018). We computed the probability density of spiking after common input arrival and the corresponding cumulative density of spiking within a given time window. Then, we obtained the probabilities of binary activity patterns of two neurons, after common input arrival. The activity patterns in the binned spike data were approximated as a mixture of two probability mass functions: The one that describes population patterns after receiving the common input, and the other that describes population patterns when there is no common input. We assessed the strength of neural interaction using the information geometric measure of correlations. Extending this scheme to three-neurons analysis, we derived triple-wise interactions of a set of postsynaptic neurons receiving common signaling input (excitatory or inhibitory) in different neural architectures (star or triangle). By doing so, we connected the synaptic inputs, membrane dynamics, threshold nonlinearity, network architecture, and also statistics of the population activity. Our results point to the possibility of inferring the underlying neuronal architectures and the type of common input, using pairwise and triple-wise neural interactions. We also showed for a specific set of data (Ohiorhenuan et al., 2010) in comparison with the analytical result, excitatory shared inputs to pairs of neurons rather than inhibition to trios can explain the data; it can be the architecture behind the observed negative triple-wise interactions.

Several studies of higher-order interactions among models of neurons reveal key features of neural activity, and suggest mechanisms underlying the observed interactions in a neural pool (Barreiro et al., 2014; Cayco-Gajic et al., 2015; Montangie and Montani, 2017; Montani et al., 2013; Shimazaki et al., 2015; Zylberberg and Shea-Brown, 2015). For example, there exist a simple model of neurons, known as the Dichotomized Gaussian (DG) model (Amari et al., 2003; Macke et al., 2009, 2011; Tchumatchenko et al., 2010); it is composed of threshold devices that receive inputs sampled from a correlated multivariate Gaussian distribution. The output binary patterns of this model exhibit characteristic higher-order interactions, namely positive pairwise and negative triple-wise interactions (Shimazaki et al., 2015; Yu et al., 2011), which results in the observed sparse activity (Shimazaki et al., 2015). How-

ever, it was speculated that common inhibitory inputs can also generate the same neural interactions (Ohiorhenuan and Victor, 2011; Shimazaki et al., 2015). Hence, the plausibility of these two scenarios in different network architectures remained to be studied. The DG model based on the Gaussian approximation for common synaptic inputs (Amari et al., 2003; Leen and Shea-Brown, 2015; Macke et al., 2011; Montangie and Montani, 2015) as well as extended DG model for non-Gaussian inputs (Barreiro et al., 2014; Montangie and Montani, 2017, 2018) are limited in investigating the outcome of these two different architectures. DG models do not incorporate the dynamics of synapses and membrane potentials, and are not suitable for investigating types of synaptic inputs in different architectures. Here, we tried to fill the gap by introducing a quantitative analytic method that links intrinsic membrane dynamics, structure and strength of common inputs, and nonlinearity of input-output neural spiking, to the spiking statistics and interactions among neurons.

Using our analytical solution, we clarified that: (i) positive pairwise and negative triple-wise interactions are produced if either each pair of neurons receive common excitatory input (triangular architecture with common excitatory input) or if all neurons receive common inhibitory input (star architecture with common inhibitory input); (ii) interaction values are significantly weaker when all neurons receive common inhibitory input; (iii) the two scenarios are clearly distinguishable in the plane of pairwise and triple-wise interaction values within the physiological ranges of parameters we examined (see Fig 5C and Fig 6B). Parallel to our analytical results using the regularly applied common inputs, we performed a set of simulations in which we apply Poisson common inputs. The results mentioned above are also reconfirmed in these simulations.

According to (i), to explain the observed positive pairwise and negative triple-wise interactions, we expect that excitatory signaling inputs are shared by two but not by more neurons, or inhibitory inputs are shared by at least three neurons. This scenario is consistent with the observed sparse connections among excitatory neurons (Holmgren et al., 2003; Ikegaya et al., 2013; Lefort et al., 2009) and also suggests dense inhibitory to excitatory connections observed in some experimental studies (Fino and Yuste, 2011; Packer and Yuste, 2011). Based on (ii), the interactions are considerably weak when neurons receive inhibitory inputs. Therefore sufficiently strong negative triple-wise interactions observed in the experiments (Ohiorhenuan et al., 2010; Ohiorhenuan and Victor, 2011; Shimazaki et al., 2015; Yu et al., 2011) are not likely to be reproduced by only common inhibitory inputs to trios. Shared excitatory inputs to pairs can reproduce the strong negative triple-wise interactions. This result implies that the synaptic architecture where excitatory inputs are sparsely shared across neurons is prevalent in some neural systems.

Besides, (iii) suggests that one can identify the underlying architecture and type of common input (excitation or inhibition) if the higher-order interactions are obtained with sufficient accuracy. Using our exact solution of the LIF model, we showed that the triangular and star architectures have distinct signatures in the pairwise and triple-wise interaction plane; this makes identification of these two architectures possible. Investigating experimental data of (Ohiorhenuan and Victor 2011, Fig 4b) in our framework (Fig 7) suggests that nearby neurons within 300 μm form excitatory triangular architecture, however for far away neurons (≥ 600 μm) no concrete suggestion can be made. The weaker interactions of the distant neurons may be due to lack of common inputs, or it can also be attributed to the heterogeneity of these neurons that cancels out interactions by mixing different architectures and types of common inputs.

Extending our method to investigate such conditions is the next step of this study.

The quantitative model we introduced here, is based on two distinct network architectures (triangle or star) with either excitatory or inhibitory shared inputs. It is interesting to see if mixtures of excitatory and inhibitory common inputs in both triangle and star architectures can lead to the observed negative triple-wise interactions. We also analyzed the model that each time two architectures are mixed. The result showed that the excitatory triangle architecture was still the prevailing architecture to generate the observed negative triple-wise interactions (data not shown here). Furthermore, in this study, we consider only feedforward connections (common inputs) and did not include inter-connections between excitatory postsynaptic neurons. The time window we consider after signal arrival is around 5ms, which is short for recurrent or feedback signal arrival which usually takes more time (two synapses or more, $15 - 20ms$) comparing with the time of stimulus onset and signal arrival. In addition, the observed sparse connectivity of pyramidal neurons (Holmgren et al., 2003; Lefort et al., 2009; Markram et al., 1997; Mizusaki et al., 2016) may support the analysis of considering common input for pyramidal neurons in the animal cortex. It is also studied in the mature animals that the pyramidal neurons in visual cortex are not interconnected (Jiang et al., 2015). However, it remains to be examined if recurrent and more complicated connections of networks change the predicted architecture for explaining the observed sparse activity.

Our theoretical method is valid for neurons with membrane potentials close to the threshold of spiking and the background noise is assumed to be Gaussian. These assumptions are motivated by the recent study (Tan et al., 2014) that shows V1 neurons operate near the threshold regime and the background noise would be uncorrelated during sensory stimulation. It would be open for future investigation to extend this method when the voltage of neuron is far from the threshold. The other assumption is that the firing rate of signaling input is low and sparse (Wolfe et al., 2010) and less than the firing rate of the postsynaptic neuron. So just one or none spike of signaling input occurs between two spikes of the postsynaptic neuron. The next step to extend this method would be to consider the cases with the high firing rate of signaling input comparing with postsynaptic neuron's rate(see Appendix III in Shomali et al. 2018).

Here, we provided a theoretical tool to predict network architecture and types of neurons (excitatory/inhibitory) from activity of neurons recorded in vivo, based on the dynamics of a standard neuron model. While it is quite challenging to perform in vivo patch clamp of common inputs and postsynaptic neurons at the same time, such an experiment that can directly identify input types and structure of the networks from living animals is helpful to improve the prediction by this method, and make it applicable to a variety of in vivo data.

Acknowledgments

H.S. thanks S.Koyama and R.Kobayashi for valuable discussions; S.RS and SN.R acknowledge T.Fukai's kind supports and are grateful to him and H.Maboudi for valuable discussions.

References

Amari, S.-i. (2001). Information geometry on hierarchy of probability distributions. Information Theory, IEEE Transactions on, 47, 1701–1711.

Amari, S.-i. (2009a). Information geometry and its applications: Convex function and dually flat manifold. In Emerging Trends in Visual Computing. (Springer), pp. 75–102.

Amari, S.-i. (2009b). Measure of correlation orthogonal to change in firing rate. Neural computation, 21, 960–972.

Amari, S.-i., Nakahara, H., Wu, S., and Sakai, Y. (2003). Synchronous firing and higher-order interactions in neuron pool. Neural computation, 15, 127–142.

Barreiro, A. K., Gjorgjieva, J., Rieke, F., and Shea-Brown, E. (2014). When do microcircuits produce beyond-pairwise correlations? Frontiers in computational neuroscience, 8, 10.

Cayco-Gajic, N. A., Zylberberg, J., and Shea-Brown, E. (2015). Triplet correlations among similarly tuned cells impact population coding. Frontiers in computational neuroscience, 9, 57.

Cover, T. M. and Thomas, J. A. (1991). Elements of information theory. (John Wiley & Sons).

Cox, D. R. (1962). Renewal theory, vol. 4. (Methuen London).

Fino, E. and Yuste, R. (2011). Dense inhibitory connectivity in neocortex. Neuron, 69, 1188–1203.

Holmgren, C., Harkany, T., Svennenfors, B., and Zilberter, Y. (2003). Pyramidal cell communication within local networks in layer 2/3 of rat neocortex. The Journal of physiology, 551, 139–153.

Hu, Y., Trousdale, J., Josic, K., and Shea-Brown, E. (2013). Motif statistics and spike correlations in neuronal networks. Journal of Statistical Mechanics: Theory and Experiment, 3, 03012.

Hu, Y., Trousdale, J., Josić, K., and Shea-Brown, E. (2014). Local paths to global coherence: cutting networks down to size. Physical Review E, 89, 032802.

Ikegaya, Y., Sasaki, T., Ishikawa, D., Honma, N., Tao, K., Takahashi, N., Minamisawa, G., Ujita, S., and Matsuki, N. (2013). Interpyramid spike transmission stabilizes the sparseness of recurrent network activity. Cerebral Cortex, 23, 293–304.

Jiang, X., Shen, S., Cadwell, C. R., Berens, P., Sinz, F., Ecker, A. S., Patel, S., and Tolias, A. S. (2015). Principles of connectivity among morphologically defined cell types in adult neocortex. Science, 350, aac9462.

Leen, D. A. and Shea-Brown, E. (2015). A simple mechanism for beyond-pairwise correlations in integrate-and-fire neurons. The Journal of Mathematical Neuroscience (JMN), 5, 17.

Lefort, S., Tomm, C., Sarria, J.-C. F., and Petersen, C. C. (2009). The excitatory neuronal network of the c2 barrel column in mouse primary somatosensory cortex. Neuron, 61, 301–316.

Macke, J. H., Berens, P., Ecker, A. S., Tolias, A. S., and Bethge, M. (2009). Generating spike trains with specified correlation coefficients. Neural computation, 21, 397–423.

Macke, J. H., Opper, M., and Bethge, M. (2011). Common input explains higher-order correlations and entropy in a simple model of neural population activity. Physical Review Letters, 106, 208102.

Markram, H., Lübke, J., Frotscher, M., Roth, A., and Sakmann, B. (1997). Physiology and anatomy of synaptic connections between thick tufted pyramidal neurones in the developing rat neocortex. The Journal of physiology, 500, 409.

Martignon, L., Deco, G., Laskey, K., Diamond, M., Freiwald, W., and Vaadia, E. (2000). Neural coding: higher-order temporal patterns in the neurostatistics of cell assemblies. Neural Computation, 12, 2621–2653.

McCormick, D. A., Connors, B. W., Lighthall, J. W., and Prince, D. A. (1985). Comparative electrophysiology of pyramidal and sparsely spiny stellate neurons of the neocortex. J Neurophysiol, 54, 782–806.

Mizusaki, B. E., Stepanyants, A., Chklovskii, D. B., and Sjöström, P. J. (2016). Neocortex: a lean mean storage machine. Nature neuroscience, 19, 643.

Montangie, L. and Montani, F. (2015). Quantifying higher-order correlations in a neuronal pool. Physica A: Statistical Mechanics and its Applications, 421, 388–400.

Montangie, L. and Montani, F. (2017). Higher-order correlations in common input shapes the output spiking activity of a neural population. Physica A: Statistical Mechanics and its Applications, 471, 845–861.

Montangie, L. and Montani, F. (2018). Common inputs in subthreshold membrane potential: The role of quiescent states in neuronal activity. Physical Review E, 97, 060302.

Montani, F., Phoka, E., Portesi, M., and Schultz, S. R. (2013). Statistical modelling of higher-order correlations in pools of neural activity. Physica A: Statistical Mechanics and its Applications, 392, 3066–3086.

Nakahara, H. and Amari, S.-i. (2002). Information-geometric measure for neural spikes. Neural Computation, 14, 2269–2316.

Ocker, G. K., Hu, Y., Buice, M. A., Doiron, B., Josić, K., Rosenbaum, R., and Shea-Brown, E. (2017a). From the statistics of connectivity to the statistics of spike times in neuronal networks. Current opinion in neurobiology, 46, 109–119.

Ocker, G. K., Josić, K., Shea-Brown, E., and Buice, M. A. (2017b). Linking structure and activity in nonlinear spiking networks. PLoS computational biology, 13, e1005583.

Ohiorhenuan, I. E., Mechler, F., Purpura, K. P., Schmid, A. M., Hu, Q., and Victor, J. D. (2010). Sparse coding and high-order correlations in fine-scale cortical networks. Nature, 466, 617–621.

Ohiorhenuan, I. E. and Victor, J. D. (2011). Information-geometric measure of 3-neuron firing patterns characterizes scale-dependence in cortical networks. Journal of computational neuroscience, 30, 125–141.

Ostojic, S., Brunel, N., and Hakim, V. (2009). How connectivity, background activity, and synaptic properties shape the cross-correlation between spike trains. Journal of Neuroscience, 29, 10234–10253.

Packer, A. M. and Yuste, R. (2011). Dense, unspecific connectivity of neocortical parvalbumin-positive interneurons: a canonical microcircuit for inhibition? The Journal of Neuroscience, 31, 13260–13271.

Pernice, V., Staude, B., Cardanobile, S., and Rotter, S. (2011). How structure determines correlations in neuronal networks. PLoS computational biology, 7, e1002059.

Rosenbaum, R., Smith, M. A., Kohn, A., Rubin, J. E., and Doiron, B. (2017). The spatial structure of correlated neuronal variability. Nature neuroscience, 20, 107.

Shadlen, M. N. and Newsome, W. T. (1998). The variable discharge of cortical neurons: implications for connectivity, computation, and information coding. The Journal of neuroscience, 18, 3870–3896.

Shimazaki, H., Amari, S.-i., Brown, E. N., and Grün, S. (2012). State-space analysis of time-varying higher-order spike correlation for multiple neural spike train data. PLoS computational biology, 8, e1002385.

Shimazaki, H., Sadeghi, K., Ishikawa, T., Ikegaya, Y., and Toyoizumi, T. (2015). Simultaneous silence organizes structured higher-order interactions in neural populations. Scientific Reports, 5, 9821.

Shomali, S. R., Ahmadabadi, M. N., Shimazaki, H., and Rasuli, S. N. (2018). How does transient signaling input affect the spike timing of postsynaptic neuron near the threshold regime: an analytical study. Journal of computational neuroscience, 44, 147–171.

Softky, W. R. and Koch, C. (1993). The highly irregular firing of cortical cells is inconsistent with temporal integration of random epsps. The Journal of Neuroscience, 13, 334–350.

Tan, A. Y., Chen, Y., Scholl, B., Seidemann, E., and Priebe, N. J. (2014). Sensory stimulation shifts visual cortex from synchronous to asynchronous states. Nature, 509, 226–229.

Tchumatchenko, T., Malyshev, A., Geisel, T., Volgushev, M., and Wolf, F. (2010). Correlations and synchrony in threshold neuron models. Physical review letters, 104, 058102.

Trousdale, J., Hu, Y., Shea-Brown, E., and Josić, K. (2012). Impact of network structure and cellular response on spike time correlations. PLoS computational biology, 8, e1002408.

Tuckwell, H. C. (1988). Introduction to Theoretical Neurobiology: Nonlinear and stochastic theories, vol. 2. (Cambridge University Press).

Vreeswijk, C. v. and Sompolinsky, H. (1996). Chaos in neuronal networks with balanced excitatory and inhibitory activity. Science, 274, 1724–1726.

Vreeswijk, C. v. and Sompolinsky, H. (1998). Chaotic balanced state in a model of cortical circuits. Neural computation, 10, 1321–1371.

Wang, M. C. and Uhlenbeck, G. E. (1945). On the theory of the brownian motion ii. Reviews of Modern Physics, 17, 323.

Wolfe, J., Houweling, A. R., and Brecht, M. (2010). Sparse and powerful cortical spikes. Current opinion in neurobiology, 20, 306–312.

Yu, S., Yang, H., Nakahara, H., Santos, G. S., Nikolić, D., and Plenz, D. (2011). Higher-order interactions characterized in cortical activity. The Journal of Neuroscience, 31, 17514–17526.

Zylberberg, J. and Shea-Brown, E. (2015). Input nonlinearities can shape beyond-pairwise correlations and improve information transmission by neural populations. Physical Review E, 92, 062707.